

High-temperature change of the creep rate in $\text{YBa}_2\text{Cu}_3\text{O}_{7-\delta}$ films with different pinning landscapesN. Haberkorn,^{1,*} M. Miura,¹ J. Baca,¹ B. Maiorov,¹ I. Usov,² P. Dowden,¹ S. R. Foltyn,¹ T. G. Holesinger,¹ J. O. Willis,¹ K. R. Marken,¹ T. Izumi,³ Y. Shiohara,³ and L. Civale¹¹*Superconductivity Technology Center, Los Alamos National Laboratory, Los Alamos, New Mexico 87545, USA*²*MST-7, Los Alamos National Laboratory, Los Alamos, New Mexico 87545, USA*³*Superconductivity Research Laboratory, International Superconductivity Technology Center, 10-13, Shinonome 1-chome, Koto-ku, Tokyo, 135-0062, Japan.*

(Received 22 February 2012; revised manuscript received 6 April 2012; published 8 May 2012)

Magnetic relaxation measurements in $\text{YBa}_2\text{Cu}_3\text{O}_{7-\delta}$ (YBCO) films at intermediate and high temperatures show that the collective vortex creep based on the elastic motion of the vortex lattice has a crossover to fast creep that significantly reduces the superconducting critical current density (J_c). This crossover occurs at temperatures much lower than the irreversibility field line. We study the influence of different kinds of crystalline defects, such as nanorods, twin boundaries, and nanoparticles, on the high-temperature vortex phase diagram of YBCO films. We found that the magnetization relaxation data is a fundamental tool to understand the pinning at high temperatures. The results indicate that high J_c values are directly associated with small creep rates. Based on the analysis of the depinning temperature in films with columnar defects, our results indicate that the size of the defects is the relevant parameter that determines thermal depinning at high temperatures. Also, the extension of the collective creep regime depends on the density of the pinning centers.

DOI: [10.1103/PhysRevB.85.174504](https://doi.org/10.1103/PhysRevB.85.174504)

PACS number(s): 74.25.Wx, 74.78.-w, 74.72.-h

I. INTRODUCTION

The study of vortex matter in high-temperature superconductors (HTS) continues to be a widely discussed topic. The vortex behavior is determined by their interactions with each other and with the material disorder, and by the thermal fluctuations. The vortex-vortex interactions are set by the intrinsic properties of the superconducting material (such as the critical temperature, the critical fields, and their anisotropy) and consequently are always the same for a given compound. In contrast, the interactions of the flux lines with material defects and crystalline imperfections that produce vortex pinning by locally depressing superconductivity depend on the nanoscale structure of each sample (the pinning landscape). As a result, the critical current density (J_c) can vary by orders of magnitude and exhibit very different dependencies on temperature (T) and magnetic field (H) for different specimens of the same superconductor. The influence of the thermal fluctuations, which are responsible for the existence of vortex liquid phases and the flux creep (the slow time decay of the supercurrents in the vortex solid phases), also depends strongly on the pinning landscape. The complexity of the effects of disorder is mainly responsible for the richness of the H - T vortex phase diagram and dynamic regimes of the cuprates. This topic was initially explored mostly on single crystals of HTS, such as $\text{Bi}_2\text{Sr}_2\text{CaCu}_2\text{O}_{8+x}$ (BSCCO)^{1,2} and $\text{YBa}_2\text{Cu}_3\text{O}_{7-\delta}$ (YBCO),^{3,4} that could be grown relatively clean and where well-defined pinning landscapes dominated by a single type of disorder could be controllably created, e.g. by particle irradiation.⁵⁻⁷

YBCO films, in contrast, typically exhibit disorder landscapes containing combinations of different kinds of defects, such as dislocations, twin boundaries (TBs), and precipitates, that tend to appear naturally during growth,⁸⁻¹⁰ thus their vortex pinning and creep phenomena are more complicated, and the present knowledge is still incomplete. Understanding vortex pinning in YBCO films has a broad scientific relevance

because it represents an extreme condition. Indeed, their J_c not only can be much larger than in YBCO single crystals;^{6,11} it can be larger than in any other known superconductor. At low T and in the absence of applied magnetic field J_c values as high as 80 to 90 MA/cm² have been reported,¹² corresponding to very high fractions $J_c/J_0 \sim 0.2-0.3$, where J_0 is the depairing critical current density that sets the maximum theoretical limit for J_c .¹³⁻¹⁶ It has been shown that the deliberate introduction of additional nanoscale defects such as nonsuperconducting nanoparticles and nanorods in YBCO films produces further enhancement of flux pinning in the presence of applied magnetic fields. The geometry of the defects has an important influence on the dependence of J_c on the field orientation. Whereas for aligned nanorods the J_c values increase preferentially for \mathbf{H} parallel to the defects, for nanoparticles the pinning is more isotropic.^{15,16} The topic is also technologically relevant, as films of the YBCO family are the central component of the second generation high-temperature superconducting wires, known as coated conductors (CC).

In YBCO, giant flux creep observed using magnetic relaxation measurements of the persistent currents has been described according to the collective vortex creep model based on the elastic properties of the vortex lattice.³ The nature of the vortex structure and the vortex pinning mechanisms can be inferred from the glassy exponent μ , which scales the effective energy barrier and the persistent current density (J) as $U(J) \approx U_c (\frac{J}{J_c})^\mu$ and depends on the creep regime. In single crystals with random point defects the temperature dependence of the creep rate ($S = -\partial \ln J_c / \partial \ln t$) shows several regimes described by collective creep theory,³ $S = -T/(U_0 + \mu T \ln t/t_0)$, where U_0 is the collective barrier in the absence of a driving force and t_0 is an effective hopping attempt time. At intermediate temperatures $U_0 \ll \mu T \ln t/t_0$, thus $S \approx -(\mu \ln t/t_0)^{-1}$ and the creep rate shows a plateau associated with glassy relaxation. Based on the model of the nucleation of vortex loops, the regime-dependent glassy exponent μ for

random point defects for the three-dimensional case is $1/7$, $3/2$ or $5/2$, and $7/9$ for single-vortex creep, small-bundle creep, or large-bundle creep, respectively.³ However, the vortex phase diagram is strongly affected by the nature (i.e. the size and shape) and the density of the pinning sites.^{3,17,18} For example, in samples with correlated disorder, new regimes appear. When $\mu_0 H$ is smaller than the matching field (B_ϕ , where the density of correlated defects equals the density of vortices), the creep rate shows a peak at temperatures around 30 K and a drop in J_c that is associated with double-kink excitations.^{3,19,20} For $\mu_0 H < B_\phi$ each vortex is individually pinned by a single defect, and double-kink excitations are possible, whereas for $\mu_0 H > B_\phi$, the fraction of vortices B_ϕ/B is firmly pinned by correlated defects, whereas the rest are merely fixed by the shear force of the vortex lattice.¹⁰ For all types of pinning sites, at high enough temperatures, the collective creep disappears, and the vortex dynamics become faster, with a dramatic drop in the J_c values.^{21,22}

Although the vortex pinning and creep regimes in YBCO films are similar to those initially discussed for single crystals, clear differences have also been observed.^{9,15,23} Large J_c improvements have been made possible by the knowledge of the influence of the shape, size, density and distribution of the defects on the dependence of vortex pinning on T and \mathbf{H} , but systematic comparative studies of the influence of the different pinning landscapes on the $S(H,T)$ and $J_c(H,T)$ diagrams have not been performed for YBCO films. More fundamental research is still needed to guide further progress, particularly at high temperatures in the range of liquid N_2 , where the effective J_c is strongly reduced by the fast flux creep associated with large thermal fluctuations. This is a serious limitation in CC performance, resulting in extended regions in the H - T plane below the irreversibility line, where J_c is nonetheless too small for practical applications.

In this paper, we explore and discuss the influence of the type (aligned-columnar or randomly distributed nanoparticles), size, and density of pinning centers on the high-temperature slow-to-fast creep rate crossover. We analyze the $S(T,H)$ phase diagram and the correlation with the resulting $J_c(H)$, and discuss the possibility to improve J_c by extending the collective creep regime to higher temperatures, with the consequent reduction of the creep rate.

II. EXPERIMENTAL

The film dimensions are defined as: length l , width, w ($w < l$); and thickness t (c axis parallel to t). The magnetization (\mathbf{M}) measurements were performed using a superconducting quantum interference device (SQUID) magnetometer for two applied magnetic field (\mathbf{H}) configurations: \mathbf{H} parallel to the c axis ($\mathbf{H} \parallel c$) and \mathbf{H} rotated (along an axis parallel to l) by an angle $\Theta = 45^\circ$ from the c axis ($\mathbf{H} \parallel 45^\circ$). The J_c values were calculated from the magnetization data using the appropriate geometrical factor in the Bean Model.²⁴ The creep measurements [$J_c(t)$, where t is time] were recorded over a period of 1 h. The initial time was adjusted to give the best correlation factor in the log-log fitting of the $J_c(t)$ dependence. The critical state for each measurement was generated using a ΔH of $\sim 4 H^*$, where H^* is the first magnetic field for full-flux penetration.⁴

Measurements were performed on four well-characterized YBCO films: (1) Y-CD-SA: a YBCO film with $t \sim 0.54 \mu\text{m}$ and columnar defects (CDs) parallel to the c axis introduced by self-assembly. The film was grown on (100) SrTiO_3 by pulsed laser deposition (PLD) from a target with YBCO + 5(mol)% Y_2O_3 + 2.5% YBa_2ZrO_3 + 2.5% YBa_2NbO_5 . The T_c in this film is ~ 90 K. Transmission electron microscopy (TEM) images show the presence of CDs with typical diameters of 6 nm, aligned parallel to the c axis with $B_\phi \sim 2$ T. (2) Y-CD-Irr: YBCO film with $T_c \sim 90$ K, $t \sim 1 \mu\text{m}$, and CDs parallel to the c axis introduced by irradiation⁶ with 600 MeV Xe with a dose equivalent to a $B_\phi \sim 2$ T. The film was grown by PLD on (100) SrTiO_3 ,²⁵ CDs produced by irradiation with 600 MeV Xe have typical diameters of 5 nm. (3) Y-NP-225: YBCO film with $t \sim 0.5 \mu\text{m}$ grown by metallic organic deposition (MOD). (4) YG-NP-BZO: $\text{Y}_{0.77}\text{Gd}_{0.23}\text{Ba}_2\text{Cu}_3\text{O}_{7-\delta}$ film with a thickness of $0.5 \mu\text{m}$ with BaZrO_3 nanoparticles dispersed in a film grown by MOD. The details of the sample preparation of Y-NP-225 and YG-NP-BZO have been published elsewhere,²⁶ and the structural and superconducting properties of these samples were previously discussed.¹⁶ Both films have large $\text{RE}_2\text{Cu}_2\text{O}_5$ (225) precipitates; the average density of these nanoparticles was found to be $n_{225} = 0.1 \times 10^{21} \text{m}^{-3}$ for both the Y-NP-225 and YG-NP-BZO films, and $n_{\text{BZO}} = 3.7 \times 10^{21} \text{m}^{-3}$ in the YG-NP-BZO film. The size of the 225 precipitates ranged

TABLE I. Summary of the sample properties discussed in this work.

Sample	Y-CD-SA	Y-CD-irr	Y-NP-225	YG-BZO
Deposition method	Pulsed laser deposition (PLD)	PLD	Metal organic deposition (MOD)	MOD
Thickness	0.54 μm	1 μm	0.5 μm	0.5 μm
Strong pinning centers	Columnar defects by self-assembly $B_\phi \approx 2$ T Diameter ($d \approx 6$ nm)	Columnar defects by heavy ion irradiation $B_\phi \approx 2$ T $d \approx 5$ nm	$\text{RE}_2\text{Cu}_2\text{O}_5$ (225) nanoparticles density $\approx 0.1 \times 10^{21} \text{m}^{-3}$ $d \approx 80$ nm Twin boundaries ($B_\phi \approx 1.3$ T)	225 nanoparticles density $\approx 0.1 \times 10^{21} \text{m}^{-3}$ $d \approx 80$ nm Twin boundaries ($B_\phi \approx 1.9$ T)
$J_c(H=0)$				
5 K	45 MA cm^{-2}	27 MA cm^{-2}	40 MA cm^{-2}	56 MA cm^{-2}
65 K	5.9 MA cm^{-2}	3.6 MA cm^{-2}	7.5 MA cm^{-2}	11 MA cm^{-2}
75 K	3 MA cm^{-2}	1.75 MA cm^{-2}	3.8 MA cm^{-2}	6 MA cm^{-2}

from 74.4 to 100 nm with a modal particle size of 86.2 nm for both MOD films. The BZO nanoparticle size varied from 18 to 28 nm with a modal size of 23 nm.¹⁶ Both films also have a high density of TBs. The B_ϕ values resulting from the TBs were estimated from plan view TEM images, and were ~ 1.3 and ~ 1.9 T for Y-NP-225 and YG-NP-BZO, respectively.^{27,28} The main characteristics of the films are summarized in Table I.

III. RESULTS

Figure 1 shows $S(T)$ at $\mu_0 H = 0.3$ T. All the films have a peak in the $S(T)$ dependence at $T \sim 25$ K, which can be related to double-kinks expansion of the vortices from c axis correlated disorder.⁵ The observation of the double-kinks peak indicates the presence of correlated disorder in all the films, which in the case of Y-NP-225 and YG-NP-BZO points to nonnegligible pinning by TBs at low temperatures.¹⁶ Besides, the similarity in the S values between Y-CD-Irr and Y-CD-SA indicates that CDs obtained by two different mechanisms produce the same kind of pinning. In all the samples, $S(T)$ shows a plateau at intermediate temperatures that, depending on the extension of the double-kink peak [see Fig. 2(a)], starts at around 30 K. In all cases, the plateau corresponds to a small region of temperature, and the S values depend on the kind of defects present in the films. At 40 K and $0.3 \leq \mu_0 H \leq 1$ T, the creep rates at the plateau are $S^{\text{Y-CD-Irr}} \sim 0.028$, $S^{\text{Y-CD-SA}} \sim 0.028$, $S^{\text{Y-NP-225}} \sim 0.024$, and $S^{\text{YG-NP-BZO}} \sim 0.017$. By using $S = -(\mu \ln \frac{t}{t_0})^{-1}$ and a reasonable estimate of $\ln(t/t_0) \sim 30$, the μ values can be estimated as $\mu^{\text{Y-CD-Irr}} \sim \mu^{\text{Y-CD-SA}} \sim 1.2$, $\mu^{\text{Y-NP-225}} \sim 1.4$, and $\mu^{\text{YG-NP-BZO}} \sim 2$. These μ values are in the range for collective vortex creep of small bundles.³ However, to our knowledge, there are no theoretical predictions of μ values for pinning dominated by random nanoparticles or synergistic combinations of defects. Although theoretical models provide a small set of discrete μ values (constant for each regime), experimental studies on YBCO usually present a gradual evolution of μ from small to large bundles as H is increased.²⁹

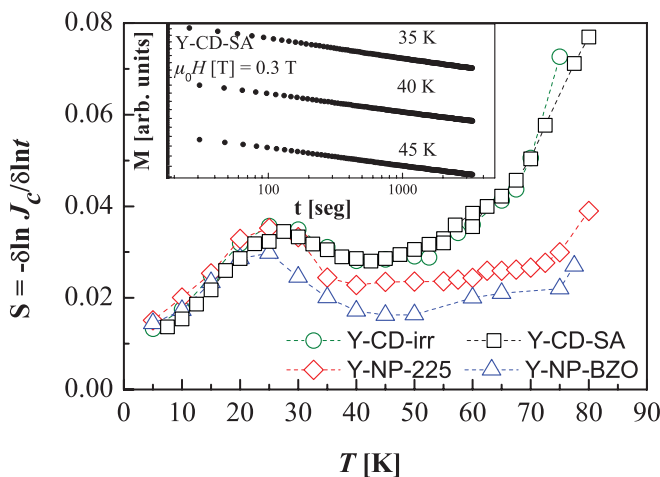


FIG. 1. (Color online) Temperature (T) dependence of the creep rate (S) in the four studied films at $\mu_0 H = 0.3$ T. Inset shows a typical set of relaxation curves in Y-CD-SA.

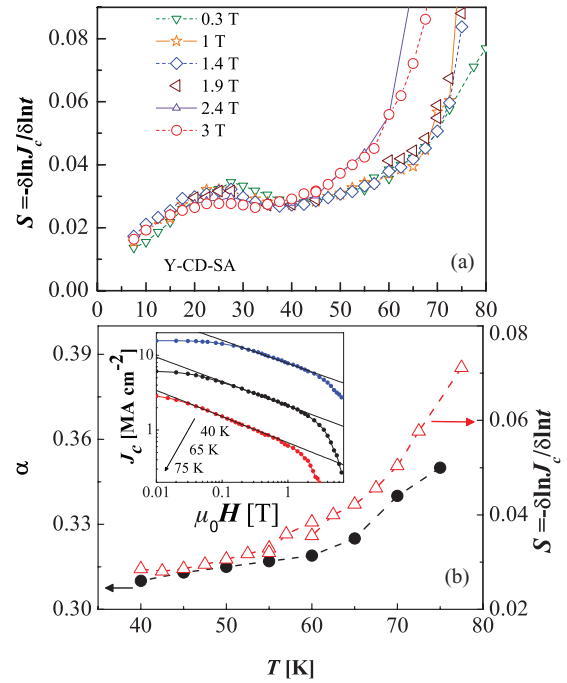


FIG. 2. (Color online) (a) Temperature dependence of the creep rate (S) at different applied magnetic fields $\mathbf{H} \parallel c$ axis in the Y-CD-SA film. (b) Correlation between $\alpha(T)$ values obtained from the J_c vs $H^{-\alpha}$ dependence (see inset) and the $S(T)$ ($\mu_0 H < B_\phi$) values of the power-law dependence.

The matching field effects on the vortex dynamics are clearly visible in Fig. 2(a), which shows $S(T)$ for Y-CD-SA at various fields with $\mathbf{H} \parallel c$ axis. First, the double-kink peak tends to disappear above B_ϕ . This was previously investigated in Ref. 11 and will not be discussed in this paper, which is instead focused on the high-temperature vortex dynamics. At temperatures higher than 40 K, where the effective flux pinning in YBCO films drops due to thermal activation, as discussed by Albrecht *et al.*,²³ the vortices remain collectively pinned in the CD. In this regime, $S(T)$ is field independent for $\mu_0 H < B_\phi$ and shows a rather abrupt increase for $\mu_0 H > B_\phi$ due to the faster dynamics of the vortices not pinned by the tracks. Figure 2(b) shows the correlation between S and $J_c(H)$ for $T \geq 40$ K. At a fixed temperature and $\mu_0 H < B_\phi$, we observe power-law behavior in $J_c(H) \propto H^{-\alpha}$.³⁰ When $\mu_0 H < B_\phi$, all the vortices are pinned inside tracks. An increase in the temperature produces an increase in thermal fluctuations resulting in an increase in the vortex-vortex interaction and a decrease in the effective pinning energy, which is manifested in an increase in the S and α values.

Figures 3(a) and 3(b) show $S(T, H)$ for Y-CD-Irr and YG-NP-BZO at $T > 40$ K. The behavior of Y-CD-Irr [Fig. 3(a)], as we described above, is similar to that found in Y-CD-SA. The only difference is the observation of a smooth increase in S with H for $\mu_0 H < B_\phi$. The reason for this difference is that the irradiation with heavy ions produces parallel CDs distributed totally randomly in the plane, thus some tracks are very close to each other or even overlap, resulting in a broad distribution of effective pinning energies. In contrast, the transversal separation among the BZO nanorods is more

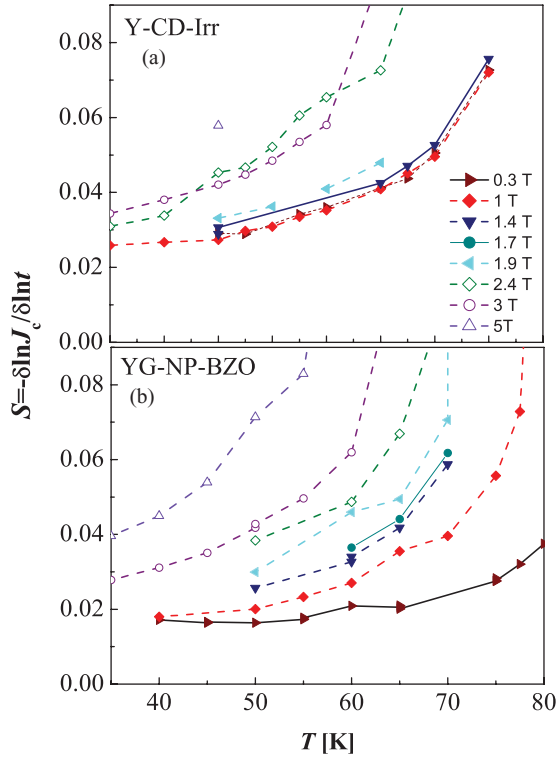


FIG. 3. (Color online) (a) and (b) Temperature dependence of the creep rate (S) at $T > 40$ K with different applied magnetic fields $\mathbf{H} \parallel c$ axis for Y-CD-Irr and YG-NP-BZO, respectively.

uniform (i.e. they are a closer analogy to the ordered lattice of CDs that produces a Mott insulator phase, although of course they lack orientational order), thus the effective pinning energies are more uniform, and the change in dynamics at B_ϕ is sharper. The $S(T, H)$ behavior for YG-NP-BZO is different from that found in films with CDs [Fig. 3(b)]. We do not observe the matching field effect in YG-NP-BZO film, which is in agreement with the expectations for strong pinning dominated by large nanoparticles. Besides, the S values at $\mu_0 H < 1$ T are smaller than in samples with CDs, which, as we will discuss later, is consistent with strong pinning and larger J_c values in this sample.¹⁶ On the other hand, at low magnetic fields, the large defects (nanoparticles) suppress the thermal smearing at $T > 40$ K, and the plateau extends to higher temperatures than in samples with CDs. As we will discuss later, we associate these differences in the extension of the plateau with the defect size, and the value of the creep rate at high temperature is directly correlated with the resulting J_c .

Figure 4 shows the H dependence of $J_c/J_c(H=0)$ and $S(H)$ at 65 K with $\mathbf{H} \parallel c$ axis and $\mathbf{H} \parallel 45^\circ$ for the films studied here. For simplification of the figure and given that the samples with CDs have the same behavior, the data for Y-CD-SA were not included. Similar features of the magnetic field (H) dependence of $J_c/J_c(H=0)$ and S were observed at 75 K, and the main results are summarized in Fig. 5. The self-field J_c ($\mathbf{H} \parallel c$ axis, 65 K) values in the different films are: Y-CD-SA: ~ 5.9 MA cm⁻² ($S \sim 0.0195$), Y-CD-Irr ~ 3.6 MA cm⁻² ($S \sim 0.022$), Y-NP-225 ~ 7.5 MA cm⁻² ($S \sim 0.016$), and YG-NP-BZO ~ 11 MA cm⁻² ($S \sim 0.014$). The J_c and S values show a direct correlation: higher J_c values are associated with

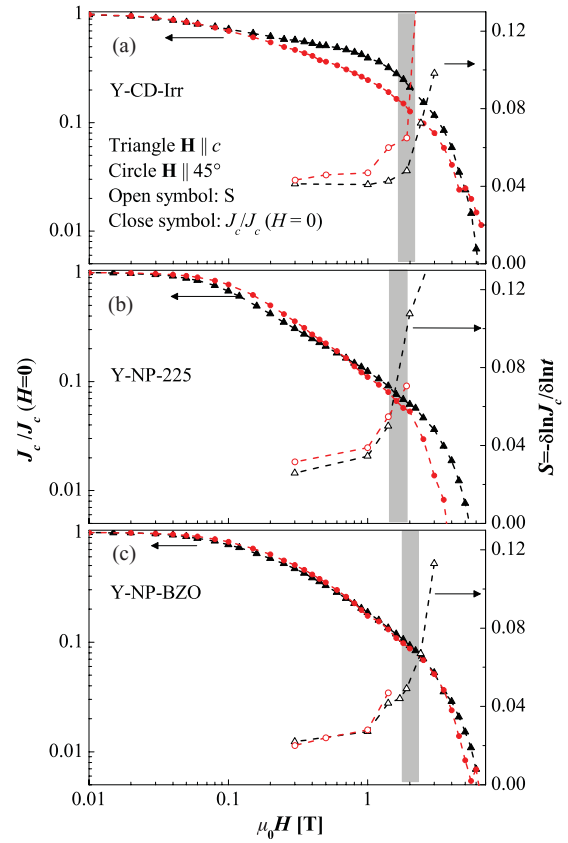


FIG. 4. (Color online) Magnetic field (H) dependence of $J_c/J_c(H=0)$ and S at 65 K for $\mathbf{H} \parallel c$ axis and $\mathbf{H} \parallel 45^\circ$. (a) Y-CD-Irr, (b) Y-NP-225, and (c) YG-NP-BZO.

smaller S values. On the other hand, the differences in the J_c values for the films with CDs (Y-CD-SA and Y-CD-Irr) can be associated with a thickness dependence of J_c ⁸ or with small differences in the diameter of the CDs. The $J_c(H)$ dependence

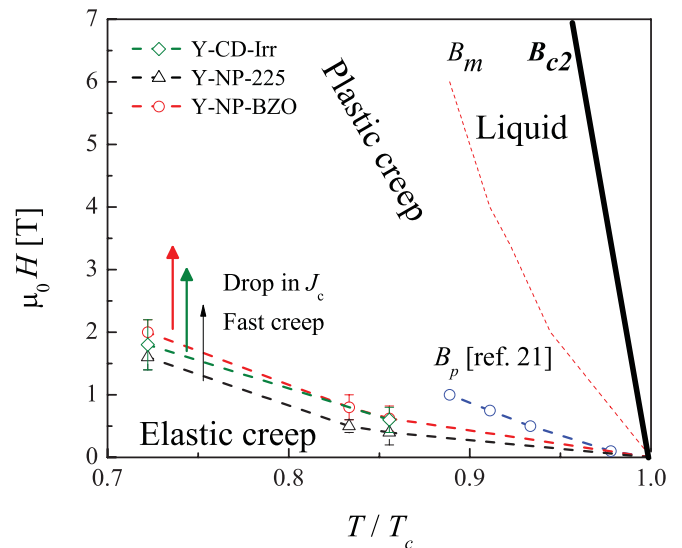


FIG. 5. (Color online) Temperature (T) dependence of the magnetic field (H) for fast creep crossover (rapid drop of J_c). The elastic-to-plastic crossover (B_p) from Ref. 21 is also shown. A tentative melting line (B_m) from Ref. 43 was also included.

of the three samples shows three clearly different regimes. The first regime between 0 and B^* , where $J_c \sim \text{constant}$, is usually associated with single vortex pinning, although it may also be affected by self-field effects.^{3,17,31,32} The second regime shows power-law behavior $J_c \propto H^{-\alpha}$,^{17,30,33–35} and finally, in the third regime the J_c starts to drop quickly. In all cases, regardless of the nature of the disorder and the field orientation, there is a clear coincidence between the crossover from the second to the third regime in J_c and a sharp increase in $S(H)$. As we discussed for Fig. 2(b), in the cases of the samples with CDs, the extension of the collective regime is associated with B_ϕ . The lower J_c values in Y-CD-Irr in comparison with the other samples can be associated with the influence of the thermal smearing on pinning, which induces a fast creep rate (see discussion below). The behavior with $\mathbf{H} \parallel 45^\circ$ is different; $\alpha \sim 0.5$ and there is a small range of magnetic field where $S \sim \text{constant}$. This result indicates that correlated disorder assists the pinning when $\mathbf{H} \parallel 45^\circ$ because each vortex is partially pinned in short segments that are aligned with the CDs.³⁶ In Y-NP-225, as was discussed in Ref. 16, TBs assist the pinning at low temperatures. However, the effect of this correlated disorder is smaller at higher temperatures, as is evident from the comparison of $J_c(H)$ and $S(H)$ for $\mathbf{H} \parallel c$ and $\mathbf{H} \parallel 45^\circ$ [see Fig. 4(b)]. In YG-NP-BZO, the absence of pinning by correlated disorder is manifested by a large α value (~ 0.7). The large J_c value at self-field in comparison with samples with CDs can be associated with the synergistic combination of large 225 precipitates and TBs.^{15,16} On the other hand, the low defect density is manifested in a small crossover magnetic field to fast creep. Finally, YG-NP-BZO shows a narrower H range where an α value can be identified, which is consistent with previous results for films with pinning by nanoparticles where a nonpower-law dependence was observed.^{15,37} The absence of a clear power-law dependence is consistent with the smooth $S(H)$ evolution presented in Fig. 3(b). The absence of correlated disorder is also evident in the similarity of $J_c(H)$ for both H configurations. On the other hand, as we will discuss later, one thing that is clear in the comparison between the Y-NP-225 and YG-NP-BZO samples is that the magnetic field at the crossover to fast creep is higher in YG-NP-BZO, indicating the effect of the high density of nanoparticles on the J_c values for this sample.

IV. DISCUSSION

Our results show that the main reason for the fast reduction of J_c in YBCO thin films at high temperatures is the increase of the creep rate S . The extension of the H - T range of the elastic creep region can be tuned by the kind, density, and size of engineered defects. Figure 5 shows a summary of the temperature dependence of the crossover to fast creep for $\mathbf{H} \parallel c$. Data from Ref. 21 indicating the elastic-to-plastic crossover in YBCO single crystals with fishtails is also included. All the samples presented in this study show a crossover to fast creep at $\mu_0 H$ values smaller than that of the plastic crossover reported for single crystals and a value much smaller than the irreversibility line (B_m), indicating that there is a large region in the H - T diagram where it is possible to enhance J_c by reducing the creep rate. The fact that the crossover to fast creep can be moved clearly motivates the systematic study of samples

with different densities and geometries of pinning centers. The differences in the elastic-to-plastic crossover between a single crystal and the films need a careful analysis. The pinning at high temperatures in YBCO single crystals is given by the combination of different kind of defects,^{3,38} which include strong and weak pinning centers. When the magnetic field is increased and the density of strong pinning centers is not enough to pin all the vortices, then $J_c(H)$ is given by the high density of random point defects that always are present in real samples. Similar behavior has been observed in YBCO³⁷ and iron-based superconductors.³⁹ At high temperatures, and in absence of strong pinning centers, $J_c(H) \sim \text{constant}$ for several Teslas, and finally starts to drop due to the influence of high thermal fluctuations. However, the J_c values given by collective pinning by random defects are much smaller than the values supported by strong pinning in thin films. We think that more studies are necessary in order to clarify this point; in particular, the intrinsic crossover to fast creep given by thermal fluctuation deserves further analysis. In all the films analyzed in this study, we observe the influence of strong pinning centers and the crossover to fast creep at H much smaller than the intrinsic limit.

Although the pinning by CDs decreases when the magnetic field is rotated,¹⁵ the analysis in the films with CDs is fundamental to the understanding of the different pinning mechanisms and their influence on the resulting J_c values. From a purely geometric point of view, the pinning mechanism should change when the $\sqrt{2}\xi = r_d$, where r_d is the radius of the defect.³ The same argument could be extended to films with nanoparticles, where short segments of the vortex are trapped.^{17,18} Making use of the temperature dependence of $\xi(T)$, the crossover temperature (T_{cr}) for strong pinning is given by $\frac{T_{cr}}{T_c} = 1 - \frac{2\xi^2(0)}{r_d^2}$;³ however, the pinning energies at higher temperatures are strongly renormalized by the thermal fluctuations, and a careful analysis is necessary. When the temperature is increased, the vortices remain in the ion tracks, and the depinning temperature in samples with CDs is given by $T_{dp} \approx T_c(v/(1+v))$, with $v = (r_d 4\xi_{ab}(0))(1/\sqrt{Gi})$.^{3,40} For YBCO, the Ginzburg number is $Gi \sim 10^{-2}$, and $\xi = 1.2$ nm.³ Using $r_d = 3$ nm, we estimate a theoretical value $T_{dp} \sim 77$ K, which is consistent with our experimental result where the vortices remain in the CDs up to 70 K. On the other hand, the crossover line to fast creep in samples with CD does not extrapolate to T_c (see Fig. 5); the crossover line should present a sharp transition in the vortex dynamics in the T_{dp} . At higher temperatures, when the thermal amplitude $\langle u^2(T) \rangle^{1/2}$ is of the order of the CD spacing, the vortex lines start to delocalize and to be pinned collectively by several columnar defects.³ The extrapolation of the last analysis to samples with nanoparticles indicates that large defects are necessary in order to avoid thermal depinning, which is consistent with a high J_c value in the film with a high density of large (23 nm) BZO nanoparticles.¹⁴ This result is consistent with previously reported data, where larger rods produce better pinning at high temperature.^{41,42}

Finally, our study shows that CDs produced by heavy ion irradiation produce pinning similar to that for self-assembled CDs, which makes it possible to explore mixed pinning landscapes in samples with a large density of nanoparticles.^{15,16}

We think that understanding the role of the defect size on the resulting $S(T, H)$ is fundamental to learning how to enhance J_c . In particular, the presence of a high density of large nanoparticles in order to extend the crossover to fast creep at high magnetic fields may considerably decrease the effective superconducting volume, reducing T_c and $J_c(0)$, and putting an upper limit on the extension to large magnetic fields of the collective creep regime in samples with large nanoparticles.

V. CONCLUSION

In conclusion, we have demonstrated that the study of the creep rate at high temperatures is a fundamental tool to understand and optimize the $J_c(H)$ values of YBCO films. We analyzed the crossover between the collective regime, associated with a plateau in the $S(T)$ dependence, and the fast creep induced by thermal depinning as T increases. The analysis of the creep rate and $J_c(T, H)$ in films with correlated

disorder allows one to understand the influence of the matching field and the diameter of pinning centers on the resulting vortex dynamics, indicating that the extension of the collective creep regime can be tuned by the manipulation of the pinning landscape. The summary presented in Fig. 5 shows that there is a large range between the crossover fields and the irreversibility line where the pinning could be improved.

ACKNOWLEDGMENTS

Research at LANL was supported by the US Department of Energy, Office of Basic Energy Sciences, Division of Materials Sciences and Engineering (magnetometry, irradiation, data analysis, manuscript preparation). Work at ISTEC-SRL (fabrication of MOD films) was supported by NEDO as Collaborative Research. N.H. is member of CONICET Argentina.

*nhaberk@cab.cnea.gov.ar

¹R. Cubitt, E. M. Forgan, G. Yang, S. L. Lee, D. McK. Paul, H. A. Mook, M. Yethiraj, P. H. Kes, T. W. Li, A. A. Menovsky, Z. Tarnawski, and K. Mortensen, *Nature* **365**, 407 (1993).

²S. Ryu, A. Kapitulnik, and S. Doniach, *Phys. Rev. Lett.* **77**, 2300 (1996).

³G. Blatter, M. V. Feigel'man, V. B. Geshkenbein, A. I. Larkin, and V. M. Vinokur, *Rev. Mod. Phys.* **66**, 1125 (1994).

⁴Y. Yeshurun, A. P. Malozemoff, and A. Shaulov, *Rev. Mod. Phys.* **68**, 911 (1996).

⁵L. Civale, A. D. Marwick, M. W. McElfresh, T. K. Worthington, A. P. Malozemoff, F. H. Holtzberg, J. R. Thompson, and M. A. Kirk, *Phys. Rev. Lett.* **65**, 1164 (1990).

⁶L. Civale, A. D. Marwick, T. K. Worthington, M. A. Kirk, J. R. Thompson, L. Krusin-Elbaum, Y. Sun, J. R. Clem, and F. Holtzberg, *Phys. Rev. Lett.* **67**, 648 (1991).

⁷M. Konczykowski, F. Rullier-Albenque, E. R. Yacoby, A. Shaulov, Y. Yeshurun, and P. Lejay, *Phys. Rev. B* **44**, 7167 (1991).

⁸S. R. Foltyn, L. Civale, J. L. Macmanus-Driscoll, Q. X. Jia, B. Maiorov, H. Wang, and M. Maley, *Nat. Mater.* **6**, 631 (2007).

⁹Yu. N. Ovchinnikov and B. I. Ivlev, *Phys. Rev. B* **43**, 8024 (1991).

¹⁰D. Larbalestier, A. Gurevich, D. M. Feldmann, and Polyanskii, *Nature* **414**, 368 (2001).

¹¹J. R. Thompson, L. Krusin-Elbaum, L. Civale, G. Blatter, and C. Feild, *Phys. Rev. Lett.* **78**, 3181 (1997).

¹²J. Raittila, M. Peurla, H. Huhtinen, P. Paturi, and R. Laiho, *Physica C* **408–410**, 647 (2004); A. A. Gapud, D. Kumar, S. K. Viswanathan, C. Cantoni, M. Varela, J. Abiade, S. J. Pennycook, and D. K. Christen, *Supercond. Sci. Technol.* **18**, 1502 (2005).

¹³J. L. MacManus-Driscoll, S. R. Foltyn, Q. X. Jia, H. Wang, A. Serquis, L. Civale, B. Maiorov, M. E. Hawley, M. P. Maley, and D. E. Peterson, *Nat. Mater.* **3**, 439 (2004).

¹⁴J. Gutierrez, A. Llordes, J. Gazquez, M. Gibert, N. Roma, S. Ricart, A. Pomar, F. Sandiumenge, N. Mestres, T. Puig, and X. Obradors, *Nat. Mater.* **6**, 367 (2006).

¹⁵B. Maiorov, S. A. Baily, H. Zhou, O. Ugurlu, J. A. Kennison, P. C. Dowden, T. G. Holesinger, S. R. Foltyn, and L. Civale, *Nat. Mater.* **8**, 398 (2009).

¹⁶M. Miura, B. Maiorov, S. A. Baily, N. Haberkorn, J. O. Willis, K. Marken, T. Izumi, Y. Shiohara, and L. Civale, *Phys. Rev. B* **83**, 184519 (2011).

¹⁷C. J. van der Beek, M. Konczykowski, A. Abal'oshev, I. Abal'osheva, P. Gierlowski, S. J. Lewandowski, M. V. Indenbom, and S. Barbanera, *Phys. Rev. B* **66**, 024523 (2002).

¹⁸A. E. Koshelev, A. B. Kolton, *Phys. Rev. B* **84**, 104528 (2011).

¹⁹L. Civale, L. Krusin-Elbaum, J. R. Thompson, R. Wheeler, A. D. Marwick, M. A. Kirk, Y. R. Sun, F. Holtzberg, and C. Feild, *Phys. Rev. B* **50**, 4102 (1994).

²⁰D. Niebieskikwiat, A. Silhanek, L. Civale, G. Nieva, P. Levy, and L. Krusin-Elbaum, *Phys. Rev. B* **63**, 144504 (2001).

²¹Y. Abulafia, A. Shaulov, Y. Wolfus, R. Prozorov, L. Burlachkov, Y. Yeshurun, D. Majer, E. Zeldov, H. Wühl, V. B. Geshkenbein, and V. M. Vinokur, *Phys. Rev. Lett.* **77**, 1596 (1996).

²²Konczykowski, A. P. Malozemoff, and F. Holtzberg, *Phys. C* **185–189**, 2203 (1991).

²³J. Albrecht, M. Djupmyr, and S. Brück, *J. Phys.: Condens. Matter* **19**, 216211 (2007).

²⁴C. P. Bean, *Phys. Rev. Lett.* **8**, 250 (1962); *Rev. Mod. Phys.* **36**, 31 (1964).

²⁵S. R. Foltyn, P. N. Arendt, Q. X. Jia, H. Wang, J. L. MacManus-Driscoll, S. Kreiskott, R. F. DePaula, L. Stan, J. R. Groves, and P. C. Dowden, *Appl. Phys. Lett.* **82**, 4519 (2003).

²⁶M. Miura, T. Kato, M. Yoshizumi, Y. Yamada, T. Izumi, Y. Shiohara, and T. Hirayama, *Appl. Phys. Express* **2**, 023002 (2009).

²⁷K. Shibata, M. Maki, T. Nishizaki, and N. Kobayashi, *Physica C: Superconductivity* **392–369**, 323 (2003).

²⁸T. Naito, H. Iwasaki, T. Nishizaki, and N. Kobayashi, *Phys. Rev. B* **70**, 014515 (2004).

²⁹J. R. Thompson, Y. R. Sun, D. K. Christen, L. Civale, A. D. Marwick, and F. Holtzberg, *Phys. Rev. B* **49**, 13287 (1994).

³⁰B. Dam, J. M. Huijbregtse, F. C. Klaassen, R. C. F. van der Geest, G. Doornbos, J. H. Rector, A. M. Testa, S. Freisem, J. C. Martinez, B. Stauble-Pumpin, and R. Griessen, *Nature (London)* **399**, 439 (1999).

³¹A. O. Ijaduola, J. R. Thompson, R. Feenstra, D. K. Christen, A. A. Gapud, and X. Song, *Phys. Rev. B* **73**, 134502 (2006).

- ³²N. Haberkorn, M. Miura, B. Maiorov, G. F. Chen, W. Yu, and L. Civale, *Phys. Rev. B* **84**, 094522 (2011).
- ³³V. Vinokur, B. Khaykovich, E. Zeldov, M. Konczykowski, R. A. Doyle, and P. H. Kes, *Physica C* **295**, 209 (1998).
- ³⁴B. Maiorov, and L. Civale, *Flux Pinning and AC Loss Studies on YBCO Coated Conductors*, edited by M. P. Paranthaman and V. Selvamanickam (Nova Science Publishers, Inc., New York, 2007).
- ³⁵M. Peurla, P. Paturi, Y. P. Stepanov, H. Huhtinen, Y. Y. Tse, A. C. Bódi, J. Raittila, and R. Laiho, *Supercond. Sci. Technol.* **19**, 767 (2006).
- ³⁶R. C. Budhani, M. Suenaga, and S. H. Liou, *Phys. Rev. Lett.* **69**, 3816 (1992).
- ³⁷V. F. Solovyov, H. J. Wiesmann, L. Wu, Q. Li, L. D. Cooley, M. Suenaga, B. Maiorov, and L. Civale, *Supercond. Sci. Technol.* **20**, L20 (2007).
- ³⁸A. Oka, S. Koyama, T. Izumi, Y. Shiohara, J. Shibata, and T. Hirayama, *Jpn. J. Appl. Phys.* **39**, 5822 (2000).
- ³⁹N. Haberkorn, B. Maiorov, M. Jaime, I. Usov, M. Miura, G. F. Chen, W. Yu, and L. Civale, *Phys. Rev. B* **84**, 064533 (2011).
- ⁴⁰L. Krusin-Elbaum, L. Civale, J. Thompson, and C. Feild, *Phys. Rev. B* **53**, 11744 (1996).
- ⁴¹C. V. Varanasi, P. N. Barnes, J. Burke, L. Brunke, I. Maartense, T. J. Haugan, E. A. Stinzianni, K. A. Dunn, and P. Haldar, *Supercond. Sci. Technol.* **19**, L37 (2006).
- ⁴²P. Paturi, M. Irjala, H. Huhtinen, and A. B. Abrahamsen, *J. App. Phys.* **105**, 23904 (2009).
- ⁴³M. Miura, S. A. Baily, B. Maiorov, L. Civale, J. O. Willis, K. Marken, T. Izumi, K. Tanabe, and Y. Shiohara, *Appl. Phys. Lett.* **96**, 072506 (2010).